

Galaxies with conspicuous optical warps \star \dagger

Vladimir P. Reshetnikov,¹ Aleksandr V. Mosenkov,^{2,1,3} Alexei V. Moiseev,^{4,5}
Sergey S. Kotov,¹ and Sergey S. Savchenko¹

¹*St. Petersburg State University, 7/9 Universitetskaya nab., St. Petersburg, 199034 Russia*

²*Sterrenkundig Observatorium, Universiteit Gent, Krijgslaan 281, B-9000 Gent, Belgium*

³*Central Astronomical Observatory, Russian Academy of Sciences, 65/1 Pulkovskoye chaussee, St. Petersburg, 196140 Russia*

⁴*Special Astrophysical Observatory, Russian Academy of Sciences, Nizhnii Arkhyz, Karachaevo-Cherkesskaya Republic, 369167 Russia*

⁵*Sternberg Astronomical Institute, Moscow M.V. Lomonosov State University, Universitetskij pr., 13, Moscow, 119992, Russia*

1 October 2018

ABSTRACT

In this paper, we present results of a photometric and kinematic study for a sample of 13 edge-on spiral galaxies with pronounced integral-shape warps of their stellar discs. The global structure of the galaxies is analyzed on the basis of the Sloan Digital Sky Survey (SDSS) imaging, in the g , r and i passbands. Spectroscopic observations are obtained with the 6-m Special Astrophysical Observatory telescope. In general, galaxies of the sample are typical bright spiral galaxies satisfying the Tully-Fisher relation. Most of the galaxies reside in dense spatial environments and, therefore, tidal encounters are the most probable mechanism for generating their stellar warps. We carried out a detailed analysis of the galaxies and their warps and obtained the following main results: (i) maximum angles of stellar warps in our sample are about 20° ; (ii) warps start, on average, between 2 and 3 exponential scale lengths of a disc; (iii) stronger warps start closer to the center, weak warps start farther; (iv) warps are asymmetric, with the typical degree of asymmetry of about several degrees (warp angle); (v) massive dark halo is likely to preclude the formation of strong and asymmetric warps.

Key words: galaxies: spiral – galaxies: structure – galaxies: kinematics and dynamics

1 INTRODUCTION

According to the prevailing point of view, disc galaxies are usually highly thin and flat. This is true, but only to a certain extent. Peripheral parts of galactic discs often exhibit deviations from the united plane and demonstrate global warps. This phenomenon has been revealed in the neutral gas component, through HI observations (e.g. Sancisi 1976, Bosma 1981, Briggs 1990, Garc a-Ruiz, Sancisi & Kuijken 2002), and in a lesser extent through optical and infrared observations (e.g. S nchez-Saavedra, Battaner & Florido 1990, de Grijs 1997, Reshetnikov & Combes 1998, 1999, Schwarzkopf & Dettmar 2001, S nchez-Saavedra et al. 2003, Ann & Park 2006, Saha, de Jong & Holwerda 2009, Gujjarro et al. 2010).

Typically, warps appear in the outskirts of opti-

cal discs, and careful investigation of edge-on galaxies have revealed that a significant fraction (e.g. $\approx 50\%$ – S nchez-Saavedra, Battaner & Florido 1990, $\approx 40\%$ – Reshetnikov & Combes 1998, $\approx 50\%$ – Ann & Park 2006) of stellar discs shows integral-shape with typical amplitudes of a few degrees. This high percentage of observed warps would suggest that the majority of galaxies are warped, since the projection effects should hide large fraction of warps, whose line of nodes is perpendicular to the line of sight. Optical warps were also common in the past, with even greater amplitudes at $z \sim 1$ (Reshetnikov et al. 2002).

Several theoretical mechanisms have been proposed to explain the formation and maintenance of warped discs (e.g. Binney 1992, Kuijken & Garc a-Ruiz 2001, Sellwood 2013 and references therein). Among the proposed scenarios, discrete modes of bending in a self-gravitating disc (Toomre 1983, Sparke & Casertano 1988), misaligned dark halos (Dubinski & Kuijken 1995), galaxy interactions and accretion of satellites (e.g. Huang & Carlberg 1997, Schwarzkopf & Dettmar 2001, Kim et al. 2014), direct ac-

\star E-mail: v.reshetnikov@spbu.ru

\dagger Partly based on observations obtained with the 6-m telescope of the Special Astrophysical Observatory of the Russian Academy of Sciences.

cretion of intergalactic matter in the outskirts of galaxies (e.g. Revaz & Pfenniger 2001, van der Kruit 2007, Roškar et al. 2010), extragalactic magnetic fields (Battaner et al. 1990), and others. This large variety of proposed mechanisms and their modifications probably indicates that there is no single mechanism responsible for all observable warps in galaxies. The current situation looks like the largest warps are mostly caused by tidal distortions (Schwarzkopf & Dettmar 2001, Ann & Park 2006), whereas relatively small warps are triggered and supported by a variety of mechanisms.

Most previous studies of optical warps have been devoted to receiving a quantitative description of this phenomenon by collecting statistics for their properties and frequency depending on galaxy morphology, while thorough investigations of warped discs for individual galaxies were quite rare. (This is partly explained by the weakness of the phenomenon: warps are usually seen in the periphery of stellar discs, and their amplitudes are often small.) Some representative examples of galaxies with the detailed studies of their optical warps are M 33 (Sandage & Humphreys 1980), NGC 5907 (warp angle $\psi \approx 4^\circ$ – Sasaki 1987), Mrk 176 ($\psi \approx 19^\circ$ – Reshetnikov 1989), NGC 4013, NGC 4565, NGC 6504 (Florido et al. 1991), MCG 06-30-005 ($\psi \approx 15^\circ$ – Kemp & Meaburn 1993), UGC 3697 ($\psi \approx 22^\circ$ – Ann 2007). Stellar discs of the Milky Way (Reed 1996), LMC (Olsen & Salyk 2002), and the Andromeda galaxy (Innanen et al. 1982) were found to be also warped.

The main goal of this paper is to perform a detailed photometric and kinematic study of thirteen edge-on spiral galaxies with integral-shaped stellar discs in order to derive observational characteristics of these galaxies and their warps. This information is very important for understanding the mechanisms responsible for the generation and maintenance of these prominent galaxy features. Until now, a detailed analysis of warped galaxies has been carried out for a few objects. In this paper, we are about to make a new contribution in this area.

This paper is organized as follows. In the next section we present our sample. In Section 3, we introduce our decomposition technique, as well as the preparation and fitting of optical galaxy images. In Section 4, we describe our own spectroscopic observations. The results of our investigation are presented in Section 5. We summarize our main findings and conclusions in Section 6.

Throughout this article, we adopt a standard flat Λ CDM cosmology with $\Omega_m=0.3$, $\Omega_\Lambda=0.7$, $H_0=70 \text{ km s}^{-1} \text{ Mpc}^{-1}$.

2 THE SAMPLE

We selected our sample of galaxies based on the view of their non-flat stellar discs in the Sloan Digital Sky Survey (SDSS, Alam et al. 2015). Most of them were visually selected during the creation of the Sloan-based Polar Ring Catalogue (SPRC Moiseev et al. 2011) and the catalogue of Edge-on disc Galaxies In SDSS (EGIS Bizyaev et al. 2014). Our sample contains 13 objects and it is biased to galaxies with strong optical warps.

Selected galaxies belong to different environments – from group members to relatively isolated objects (this information is

taken from the NASA/IPAC Extragalactic Database, NED¹ hereafter). An overview of the basic properties of the sample galaxies is given in Table 1. Fig. 1 shows SDSS thumbnail images of the galaxies. Some brief notes on each object are given below.

IC 194 (UGC 1542, RFGC 439, PGC 7812) is seen almost exactly edge-on. Optical disc warping is not strong: edge-on disc tips have a barely detectable S-shape. This galaxy has no nearby bright companions, but a loose group of galaxies PPS2 136 with the close redshift is located at a projected distance of 170 kpc from IC 194 (Trasarti-Battistoni 1998).

2MFGC 6306 is classified within the framework of the GalaxyZoo project (Lintott et al. 2008, 2011), with the weighted fraction of votes out of all responses that this galaxy is edge-on $P = 0.89$. Its stellar disc looks asymmetric and warped. 2MFGC-6306 probably forms a group with three other galaxies with close redshifts – SDSS J075644.97+440536.7, CGCG 207-007, and 2MASSX J07563889+4407408.

SPRC-192 is classified as a related to polar-ring galaxies (PRGs) object (Moiseev et al. 2011). It is an early-type spiral with the visible dust lane along the disc major axis surrounded by an inclined ring-like structure. Morphologically, it is similar to the well-known polar-ring galaxy NGC 660. Obviously, if this galaxy had a higher inclination, it would look like a strongly warped spiral. The galaxy has no nearby companions of comparable sizes, but its morphology may point to a profound external perturbation or an accretion event in the past.

UGC 4591 (RFGC 1430, PGC 24674) is an edge-on spiral galaxy, a member of the group of three galaxies WBL 193 (White et al. 1999) (the brightest of them is the spiral galaxy IC 2394). The apparent disc bending starts at the half-radius of the galaxy.

MCG +06-22-041 (RFGC 1674, PGC 28776) at $z = 0.027$ is a thin late-type spiral galaxy without any presence of a bulge. It was classified in the GalaxyZoo as an edge-on galaxy ($P = 1.0$). Similar redshifts of nearby objects (elliptical galaxy CGCG 182-048 and 2MASSX J09574267+3603307, both at $z = 0.027$) suggest that MCG +06-22-041 may be in a group.

NGC 3160 (UGC 5513, PGC 29830) is one of the most interesting objects in our sample. It was classified in the GalaxyZoo as an edge-on galaxy with $P = 0.838$. NGC 3160 shows several prominent features such as strong disc warping and a contrast X-shaped structure in the central part of the galaxy. NGC 3160 is a member of the cluster of galaxies NRGb 78, with the brightest elliptical galaxy NGC 3158 at the centre.

UGC 5791 (SPRC-197, PGC 31697) is a blue peculiar galaxy for which S⁴G (Sheth et al. 2010) analysis has been done. It is the nearest galaxy in the sample. The inclination angle for this galaxy is barely measurable because of its peculiar shape. It is a pair member, together with the galaxy UGC 5798 (Peterson 1979). UGC 5791 is classified as a PRG-related object (Moiseev et al. 2011).

NGC 3753 (UGC 6602, Arp 320, SPRC-203, PGC 36016) is an interacting galaxy, marked by Moiseev et al. (2011) as an object related to PRGs. It belongs to the compact group Hickson 57 (Hickson 1982) and was included in the catalogue of nearby poor clusters of galaxies (White et al. 1999). The warped dust disc

¹ <http://ned.ipac.caltech.edu/>

has apparent edge-on orientation. The stellar disc is significantly warped and has an asymmetric view. The galaxy image gives us a hint that its structure may include a bar or an inner disc overlapping with a dust component. Two bright companions near NGC 3753 are the spiral galaxy NGC 3754 and the elliptical galaxy NGC 3750.

UGC 6882 (SPRC-204, PGC 37372) is another galaxy related to PRGs (Moiseev et al. 2011), which is probably close to edge-on orientation according to the classification from the Galaxy Zoo ($P = 0.575$). It also belongs to the 2MASS selected Flat Galaxy Catalog (2MFGC, Mitronova et al. 2004). Some small nearby galaxies are seen in the SDSS image, although they do not have optical spectra, and, thus, estimated redshifts.

SDSS J153538.63+464229.5 and **SDSS J140639.64+272242.4** are the two most distant and small in angular size galaxies in our sample. Both galaxies have several nearby companions in projection, but, unfortunately, they do not have measured redshifts.

UGC 10716 (RFGC 3242, PGC 59657) is a late-type spiral galaxy viewed almost edge-on ($P = 0.933$). It was selected in the RFGC catalogue and in the catalogue of edge-on galaxies created by Kautsch et al. (2006). The galaxy forms a triplet with UGC 10714 and SDSS J170726.32+301316.6 (Berlind et al. 2006).

UGC 12253 (RFGC 4028, PGC 70040) is seen in almost exactly edge-on orientation. The sharp dust lane divides the main body of UGC 12253 almost ideally in two halves. The X-pattern at the centre suggests that this galaxy has a boxy/peanut-shaped bulge, a possible evidence of the presence of a bar (Bureau et al. 2006). There are two nearby galaxies with close redshifts (PGC 070044 and SDSS J225556.61+124701.9) and, therefore, UGC 12253 can be a member of a triplet or a group of galaxies.

3 PREPARATION AND DECOMPOSITION OF GALAXY IMAGES

3.1 Photometric decomposition technique

An ordinary way to determine structural parameters of spiral galaxies implies performing the decomposition of their 1D- or 2D-brightness distributions into their two main components: a spherical bulge and a flat disc. The main goal of the decomposition analysis is to separate contributions of different components in the overall brightness distribution and to build a photometric model of the galaxy.

The common empirical model for the bulge representation (in mag/\square'') is the Sérsic model (Sérsic 1968):

$$\mu(r) = \mu_{0,b} + \frac{2.5 \nu_n}{\ln 10} \left(\frac{r}{r_{e,b}} \right)^{\frac{1}{n}}, \quad (1)$$

where $\mu_{0,b}$ is the central surface brightness, $r_{e,b}$ is the effective radius, and n is the so-called Sérsic index with ν_n to be a function depending on n (Caon, Capaccioli & D’Onofrio 1993).

The disc is usually described by the exponential law, which in the logarithmic scale (in mag/\square'') turns into a simple linear function of the radius (Patterson 1940; Freeman 1970):

$$\mu(r) = \mu_{0,d} + 1.086 \frac{r}{h}, \quad (2)$$

where $\mu_{0,d}$ is the disc central surface brightness and h is its exponential scale length.

The distribution of the surface brightness in the radial r and vertical z directions for the transparent “exponential” disc observed at the edge-on orientation is described by the following expression (in intensities):

$$I(r, z) = I(0, 0) \frac{r}{h} K_1 \left(\frac{r}{h} \right) \text{sech}^2(z/z_0), \quad (3)$$

where $I(0, 0)$ is the disc central intensity, h is the radial scale length, z_0 is the “isothermal” scale height of the disc (Spitzer 1942; van der Kruit & Searle 1981a; van der Kruit & Searle 1981b, 1982a,b), and K_1 is the modified Bessel function of the first order. To find the edge-on disc central surface brightness, we should calculate $I_0^{\text{edge-on}} = \int_{-\infty}^{\infty} I(r, 0) dr$. The central surface brightness reduced to the face-on is found as $I_0^{\text{face-on}} = I_0^{\text{edge-on}} z_0/h$. Further, we will use its logarithmic value $\mu_{0,d}$ in mag/\square'' .

The above and other models are implemented into many open-access software tools designed to perform photometric decomposition of galaxy images on several components: *budda* (de Souza, Gadotti & dos Anjos 2004), *GIM2D* (Simard et al. 2002), *GALFIT* (Peng et al. 2010), *IMFIT* (Erwin 2015), *DECA* (Mosenkov 2014), etc.

In our study, we will use a non-standard approach of applying genetic algorithms (GA) to find the best fit model for a galaxy (Goldberg 1989). This approach allows us to perform decomposition in a more robust way and avoid local minima of χ^2 , whereas a standard way to find an optimal model is to apply the gradient descent (Levenberg-Marquardt) or downhill simplex (Nelder-Mead) methods. Also, since genetic algorithms are random and a parameter space is vast, the fitting procedure can be repeated multiple times without resulting in the exact the same solution. This gives us an estimate of the uncertainty for the fit parameters. Other advantages and robustness of GA for decomposition of galaxy images are presented in De Geyter et al. (2013, 2014). Below we provide a brief description of GA properties used in the current work.

GA is an effective computational algorithm for searching solutions of an optimisation problem. It simulates the natural selection process and represents possible solutions of the problem as “organisms”, with “genes” as free parameters of a model. During the optimisation procedure these “organisms” evolve through “breeding” and “mutation” processes.

We use *GALFIT* (and *IMFIT* for the galaxy SPRC-192, see details in Sect. 3.3) to generate model images of the galaxies convolved with the point spread function (PSF) images (“organisms”), and find χ^2 value (the fitness which characterizes the quality of the model). χ^2 is calculated internally in *GALFIT* and *IMFIT* which take into account the mask (to ignore all objects which will affect our simple bulge/disc decomposition) and the weight images of the galaxy. The values of each gene of each organism of zero-generation are being set randomly. The ranges of possible values for each gene are chosen such that they undoubtedly overlap the true value of the corresponding model parameter. Although using the larger range decreases the rate of the method convergence, we set the parameter ranges as large as possible, to make sure that the true values of the parameters are inside these ranges. The zero generation and any further generation comprises 200 organisms. The total number of generations is chosen to be 100. To retrieve estimates of uncertainties (their lower bounds) for each free parameter,

Table 1. Basic properties of the sample galaxies.

#	Galaxy	RA	Dec	D (Mpc)	M (mag)	a (")	q	$g-r$	$r-i$	T	i (deg)
(1)	(2)	(3)	(4)	(5)	(6)	(7)	(8)	(9)	(10)	(11)	(12)
1	IC 194	02:03:05	+02:36:51	83.8	-20.88	61.9	0.25	0.75	0.51	Sb	87.3±1.2
2	2MFGC 6306	07:56:43	+44:05:49	192.0	-21.12	36.4	0.22	0.85	0.52	Sb	88.0±1.6
3	SPRC 192	08:23:01	+32:00:54	266.5	-21.93	25.7	0.37	0.75	0.46	Sab	80.0±5.1
4	UGC 4591	08:46:58	+28:14:17	91.5	-20.26	47.4	0.34	0.64	0.34	Scd	89.7±0.4
5	MCG +06-22-041	09:57:43	+36:04:09	113.3	-18.85	29.9	0.22	0.05	-0.1	Sd	89.8±0.6
6	NGC 3160	10:13:55	+38:50:34	98.2	-21.40	56.2	0.36	0.85	0.44	Sb	89.2±1.7
7	UGC 5791	10:39:27	+47:56:50	14.6	-16.68	56.3	0.43	0.31	0.16	Sc	85.0±5.0
8	NGC 3753	11:37:54	+21:58:53	124.0	-22.29	74.6	0.31	0.89	0.49	Sab	84.3±2.7
9	UGC 6882	11:54:43	+33:32:12	135.1	-20.98	43.2	0.23	0.74	0.38	Sbc	80.1±6.2
10	SDSS J140639.64+272242.4	14:06:40	+27:22:42	303.5	-20.89	24.3	0.18	0.64	0.49	—	88.6±1.3
11	SDSS J153538.63+464229.5	15:35:39	+46:42:30	271.4	-20.17	20.7	0.22	0.41	0.18	—	84.4±1.9
12	UGC 10716	17:07:44	+30:19:35	132.5	-20.61	39.9	0.23	0.66	0.41	Sb	87.9±1.3
13	UGC 12253	22:56:02	+12:45:59	101.4	-20.61	49.8	0.27	0.84	0.42	Sb	89.8±0.5

Columns:

- (1) Designation number in the sample,
- (2) first name from NED,
- (3), (4) J2000 coordinates from NED,
- (5) 3K CMB distance from NED (except for 2MFGC 6306 for which the distance was calculated from the radial velocity taken from the HyperLeda database),
- (6) absolute magnitude in the r band inside of the isophote of 25.5 mag/arcsec². Galactic extinction (according to [Schlafly & Finkbeiner 2011](#)) and K-correction (using the NED K-Correction calculator based on [Chilingarian & Zolotukhin 2012](#)) was taken into account,
- (7), (8) semi-major axis and galaxy flattening of the 25.5 mag/arcsec² isophote in the r -band,
- (9), (10) colours corrected for Galactic extinction and K-correction,
- (11) morphological type from NED. For SDSS J140639.64+272242.4 and SDSS J153538.63+464229.5, there is no morphological classification in NED or HyperLeda databases,
- (12) galaxy disc inclination (see Appendix A in [Mosenkov et al. 2015](#)). For UGC 4591 and MCG +06-22-041, we applied the first approach from [Mosenkov et al. \(2015\)](#) using the 3D disc decomposition available in the IMFIT code. Inclination estimate for UGC 5791 is found on the basis of the apparent axial ratio of the central part of the galaxy. For the remaining galaxies, we estimated the inclination by the orientation of the dust lane (the second method from [Mosenkov et al. 2015](#)).

we repeat GA ten times. The best model with minimal χ^2 is then taken as an initial guess for the subsequent GALFIT (or IMFIT) decomposition. This is done in order make the solution found by GA more precise: GALFIT and IMFIT implement the Levenberg-Marquardt algorithm which is suitable for searching the global minimum of χ^2 when a solution, found with GA, is close to the true one.

3.2 Data handling

For our photometric analysis of galaxies, we use the data release DR12 of SDSS. The corrected frames and PSF images (prefix “ps-Field”) for three g , r , i bands were retrieved directly from the SDSS Science Archive Server (SAS). Although downloaded frames have been bias subtracted and flat-fielded, we need to do some additional preparation of the galaxy images for the further decomposition and analysis of galactic warping. All the images were sky-subtracted (sky background was fitted with the 2nd polynomial), rotated (such as the plane of the galaxy would be horizontal) and cut out from the original image (the final galaxy image should have a horizontal extent of $1.5a$ and a vertical extent of $1.5b$, where a and b are the major and minor axes respectively). Foreground stars and other contaminants were detected with the Source Extrac-

tor ([Bertin & Arnouts 1996](#)), revisited by eye, and then properly masked².

3.3 Photometric decomposition

Once the data preparation is done, we can perform photometric decomposition of the sample galaxies in the g , r , and i bands. For this, we used the GA approach described in Sect. 3.1. In addition to the masks built in the previous step (Sect. 3.2), we also masked by hand some prominent features of the galaxies which could affect the results of the fitting: dust lanes, which were detected in the g band images, and disc warps at radii where the disc bending begins to appear (see Sect. 3.4).

As the r band is the deepest band in SDSS, we will mainly use the decomposition results in this band for our further analysis of the galaxy structure. However, we carried out decomposition in two other bands as well. This information is useful to estimate the model colours $g-r$ and $r-i$ of the bulge and the disc, and compare them for different galaxies. Also, the disc scale length as well

² These steps were done with the special PYTHON package <https://github.com/latrop/pipeline>.

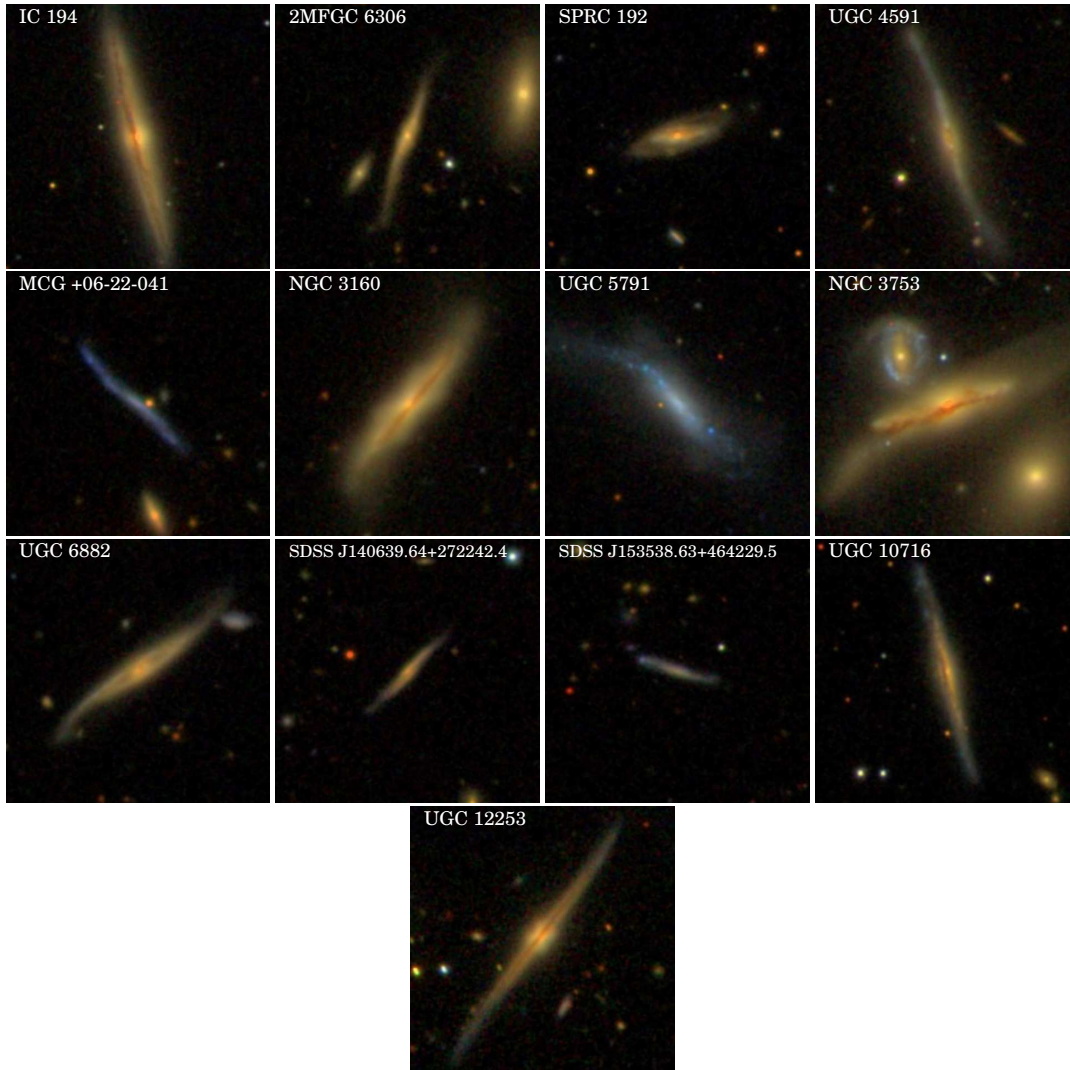


Figure 1. SDSS thumbnail images for the 13 galaxies in our sample with the field of view of $90''$ by $90''$.

as the disc scale height can be, in principal, different in different passbands, and it is interesting to compare radial colour gradients for the galaxies of the sample. Some important details on the image decomposition are given below.

All the galaxies (except UGC 6882) were fitted to the edge-on disc plus bulge model (3). The galaxy UGC 6882 looks to be not exactly edge-on, therefore for this galaxy we used an exponential non-edge-on disc model (2) with the apparent disc flattening of 0.15. However, we fitted the minor axis surface brightness distribution of this galaxy with the edge-on disc function and estimated its scale height to be $2.8''$, or 1.87 kpc. Since this galaxy is not purely edge-on, we can assume that its vertical scale is somewhat overestimated, and the found value should be used as its upper limit.

Five galaxies (UGC 4591, MCG +06-22-041, UGC 5791, SDSS J140639.64+272242.4, SDSS J153538.63+464229.5) do not exhibit the presence of a well-defined bulge, and thus they were fitted to the single disc model. SPRC-192 is a galaxy with inclined ring-like structure, for which the ring was fitted with the “Gaus-

sianRing” function using the `IMFIT` code (`GALFIT` does not offer this function). We found that the ring has the diameter of 12.6 kpc and its major axis is oriented at the angle of about 15 deg relative to the edge-on disc plane.

We should note that for the half of the galaxies the dust lane is quite prominent, and, therefore, the dust extinction can severely affect the results of our fitting. In those cases where the dust lane was masked, the model of the bulge can become unreliable since the number of unmasked pixels of the compact bulge can be significantly reduced. For this reason, we do not rely on the retrieved bulge parameters, and only investigate the disc model. The best fit parameters and their uncertainties for the r band are presented in Table 2. The bulge-to-total luminosity ratio (B/T) can be somewhat underestimated and should be used with caution.

Table 2. Structural parameters of the disc for the r -band and colours of the disc and the bulge (the D- and B-suffix respectively). The disc central surface brightness and the colours are corrected for Galactic extinction and K -correction.

#	Name	$\mu_{0,d}$ (mag/□′′)	z_0 (kpc)	h (kpc)	B/T	$(g-r)_D$ (mag)	$(r-i)_D$ (mag)	$(g-r)_B$ (mag)	$(r-i)_B$ (mag)
1	IC 194	21.98 ± 0.12	1.50 ± 0.06	6.55 ± 0.65	0.27	0.64	0.44	0.91	0.59
2	2MFGC 6306	20.71 ± 0.10	1.25 ± 0.04	3.95 ± 0.21	0.09	1.12	0.45	0.38	0.52
3	SPRC 192	20.69 ± 0.10	3.36 ± 0.10	4.84 ± 0.51	0.45	0.68	0.28	1.09	0.76
4	UGC 4591	21.22 ± 0.01	1.25 ± 0.01	3.25 ± 0.04	0.0	0.55	0.29	—	—
5	MCG +06-22-041	22.18 ± 0.02	0.65 ± 0.01	2.87 ± 0.07	0.0	0.04	-0.11	—	—
6	NGC 3160	20.62 ± 0.18	2.00 ± 0.13	4.77 ± 0.59	0.07	0.80	0.39	0.65	0.88
7	UGC 5791	21.48 ± 0.28	0.34 ± 0.04	0.66 ± 0.13	0.0	0.26	0.15	—	—
8	NGC 3753	20.70 ± 0.34	3.25 ± 0.50	7.00 ± 1.89	0.20	0.80	0.44	1.06	0.57
9	UGC 6882	22.34 ± 0.05	1.87 ± 0.49	7.15 ± 0.03	0.17	0.28	0.72	1.15	0.57
10	SDSS J140639.64+272242.4	20.17 ± 0.13	1.61 ± 0.14	5.96 ± 0.51	0.0	0.27	0.20	—	—
11	SDSS J153538.63+464229.5	20.97 ± 0.12	1.73 ± 0.11	6.15 ± 0.49	0.0	0.20	-0.13	—	—
12	UGC 10716	22.89 ± 0.13	1.18 ± 0.11	7.47 ± 0.91	0.49	0.40	0.28	1.13	0.49
13	UGC 12253	22.45 ± 0.10	1.41 ± 0.09	6.33 ± 0.63	0.37	0.71	0.38	0.89	0.41

3.4 Analysis of warps

In order to describe the structure of optical warps, we apply the following general technique to each galaxy image.

First, in each band we build an isophote map from 20.5 up to 25.5 mag/□′′ level. (Due to complex morphology of 2MFGC 6306, we use isophotal level of 24.5 mag/□′′ for it.) To plot the isophotes, we use the free astronomical application SAOImage DS9³, with the smoothness factor of 5. We verified that this smoothing does not affect the geometry of the warps. Masked pixels are excluded from the analysis.

After that, we find the center-line for each isophote using the “skeletonization” process to obtain a skeletal remnant. This topological skeleton of the isophote is equidistant to its boundaries, and therefore determines the center-line of the isophote. For this purpose we use the scikit-image⁴ collection of algorithms for image processing. All center-lines are then averaged that results in the final center-line of the galaxy, which goes from the central region to its optical outskirts.

The found center-line then can be fitted with a piecewise linear function describing three different parts of the line: left (representing the left warp of the disc), middle part (the plane of the galaxy) and the right part (the right warp of the disc). As each segment has its own slope and intercept, we can obtain two points, where the warps begin (R_w), and their orientation relative to the central segment. Here, we define the warp angle ψ as an angle measured from the galaxy centre, between the plane (middle segment of our centre-line) and line from centre to tips of the outer 25.5 isophote (see Sánchez-Saavedra, Battaner & Florido 1990, Reshetnikov & Combes 1998). As warps are not always symmetric, we calculate the warp parameters on either side of each galaxy independently. Notice here that the measurement of the warp angle is independent of how well we horizontally aligned our galaxy.

The results of the fitting are presented in Table 3 and in Fig. 2.

In Fig. 2, the galaxies are oriented in such a way that their major axes are horizontal and the north part of the galaxies is up. Signs of warp angles in Table 3 are given as follows. For left (east) halves of the galaxy images, up-bending warps have positive angles, down-bending warps have negative values. For right (west) halves, on the contrary, up-bending has negative value and down-bending is described by positive warp angles.

4 SPECTROSCOPIC OBSERVATIONS AND DATA REDUCTION

The spectroscopic observations of our sample galaxies were carried out at the prime focus of the SAO RAS 6-m telescope with the multi-mode focal reducer SCORPIO-2 (Afanasiev & Moiseev 2011), UGC 10716 was observed with the previous version of the focal reducer (SCORPIO, Afanasiev & Moiseev 2005). In the long-slit mode both devices have the same slit size (6 arcmin \times 1 arcsec) with a scale of 0.36 arcsec per pixel. The exception was UGC 5791 observed with 0.7 arcsec slit width.

The spectral resolution was similar in all cases (FWHM about 5 Å), while SCORPIO-2 provides a twice broader spectral range than old SCORPIO. The log of spectral observation is given in Table 4. The slit position was chosen along the major axis of each galaxy. For several objects we used two slit positions – along the major axis and along the tips of apparent warp.

Data reduction was performed in a standard way using the IDL software package developed at the SAO RAS for reducing the data obtained with SCORPIO/SCORPIO-2. The brightest emission lines H α and [NII] $\lambda\lambda$ 6548, 6583 were fitted by Gaussian profiles in order to calculate the ionized gas velocities along the slit. The line-of-sight velocity distributions were then converted to the galaxy rotation curves (RCs) assuming a constant disc inclination $i = 90^\circ$.

³ <http://ds9.si.edu/>

⁴ <http://scikit-image.org/>

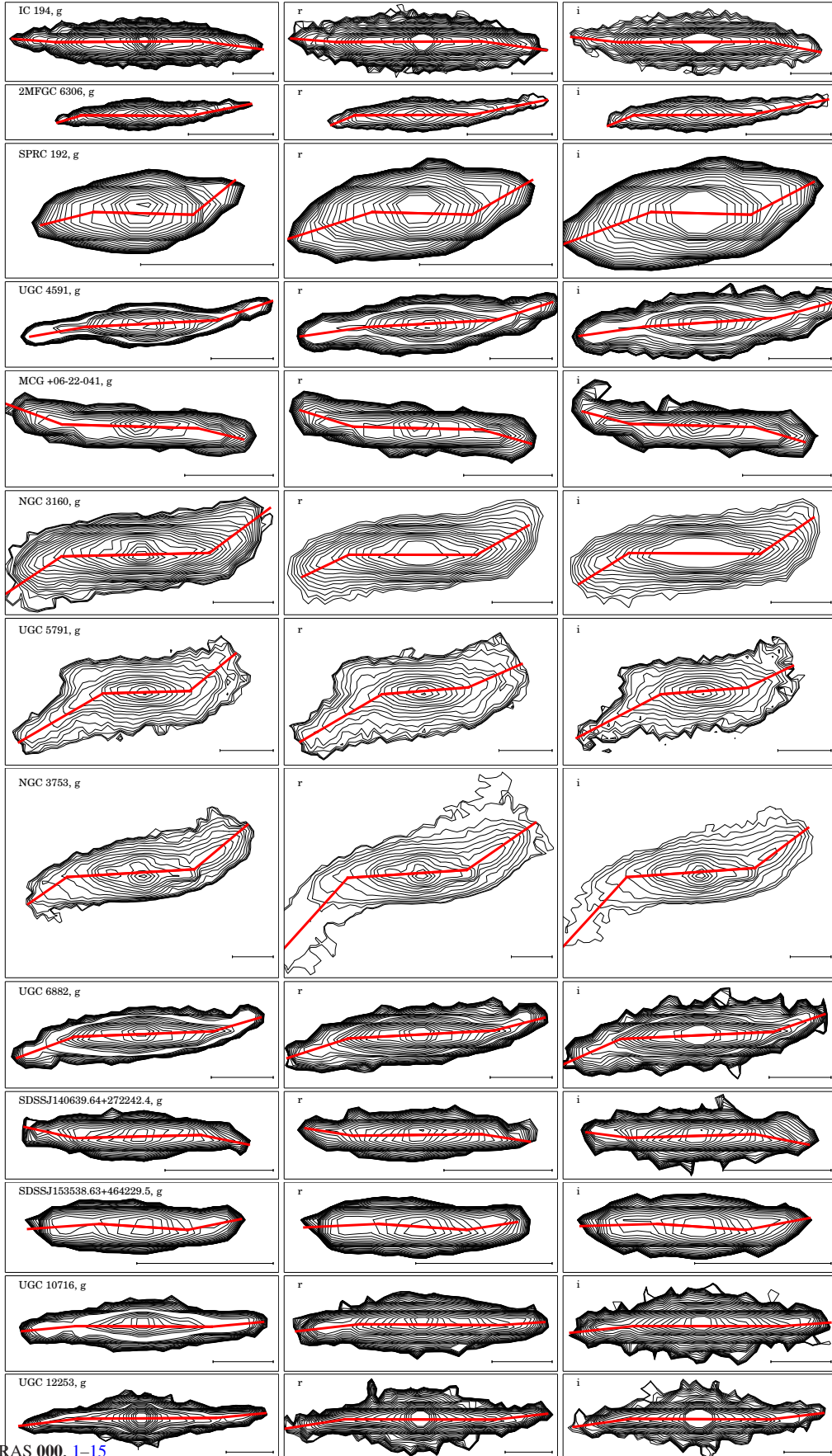


Figure 2. The g -, r - and i -band contour maps of the sample galaxies. The red line corresponds to the best fit of the center-line with the piecewise linear function. The outer isophote is of $25.5 \text{ mag}/\square''$ ($24.5 \text{ mag}/\square''$ for 2MFGC 6306). The length of the bar in the bottom right corner is $20''$.

Table 3. Warp parameters for the sample galaxies in the g , r and i bands. μ_w is the isophote level where the warp of the disc begins to appear (corrected for Galactic extinction and K-correction) which corresponds to the radius of the warp R_w in units of the disc scale length. ψ is the warp angle. “North” and “South” mean the north and south halves of galaxies.

#	Galaxy	Band	μ_w (mag/□′′)	R_w (h)	ψ (deg)	μ_w (mag/□′′)	R_w (h)	ψ (deg)
			North			South		
1	IC 194	g	23.9 ± 0.3	2.35 ± 0.04	-1.8 ± 0.2	22.3 ± 0.1	1.59 ± 0.43	4.0 ± 0.5
		r	23.2 ± 0.3	2.6 ± 0.05	-1.8 ± 0.2	21.7 ± 0.1	1.88 ± 0.49	4.1 ± 0.5
		i	22.8 ± 0.4	2.59 ± 0.05	-2.5 ± 0.3	21.4 ± 0.1	2.11 ± 0.52	5.3 ± 0.7
2	2MFGC 6306	g	22.7 ± 0.2	2.91 ± 0.12	6.2 ± 0.6	22.6 ± 0.2	2.35 ± 0.24	-4.6 ± 0.5
		r	21.9 ± 0.1	3.4 ± 0.14	7.5 ± 0.5	21.9 ± 0.1	2.98 ± 0.28	-6.3 ± 0.4
		i	21.7 ± 0.2	3.84 ± 0.14	7.2 ± 0.5	21.3 ± 0.1	2.68 ± 0.29	-6.2 ± 0.5
3	SPRC 192	g	21.7 ± 0.2	1.65 ± 0.36	5.8 ± 2.7	21.9 ± 0.4	1.75 ± 0.02	-15.9 ± 1.7
		r	21.0 ± 0.2	1.95 ± 0.41	9.8 ± 2.4	21.4 ± 0.4	2.06 ± 0.01	-13.2 ± 1.8
		i	20.7 ± 0.2	2.04 ± 0.42	13.9 ± 2.7	20.9 ± 0.3	2.15 ± 0.0	-14.2 ± 1.6
4	UGC 4591	g	22.7 ± 0.3	2.03 ± 0.09	2.1 ± 0.4	22.9 ± 0.1	2.7 ± 0.56	-6.1 ± 0.6
		r	22.3 ± 0.2	2.48 ± 0.14	1.5 ± 0.5	22.4 ± 0.1	3.29 ± 0.72	-5.4 ± 1.0
		i	21.9 ± 0.1	2.71 ± 0.16	1.4 ± 0.6	22.2 ± 0.1	3.61 ± 0.79	-5.5 ± 1.1
5	MCG +06-22-041	g	22.6 ± 0.2	3.03 ± 0.57	-9.0 ± 2.4	22.8 ± 0.4	2.12 ± 0.06	4.3 ± 0.4
		r	22.6 ± 0.2	2.94 ± 0.63	-7.4 ± 2.8	22.8 ± 0.4	2.65 ± 0.07	6.3 ± 0.6
		i	22.8 ± 0.3	3.18 ± 0.64	-6.9 ± 2.1	22.8 ± 0.5	2.47 ± 0.08	5.8 ± 0.7
6	NGC 3160	g	22.6 ± 0.2	2.4 ± 0.5	15.3 ± 3.3	22.2 ± 0.2	2.02 ± 0.06	-17.7 ± 1.7
		r	21.5 ± 0.1	2.39 ± 0.48	11.7 ± 2.7	20.9 ± 0.2	1.85 ± 0.06	-14.4 ± 1.5
		i	21.2 ± 0.1	2.19 ± 0.46	14.7 ± 2.8	20.8 ± 0.2	1.87 ± 0.06	-17.4 ± 1.7
7	UGC 5791	g	22.2 ± 0.1	1.57 ± 0.19	16.0 ± 5.8	22.6 ± 0.2	1.92 ± 0.54	-12.8 ± 3.3
		r	21.9 ± 0.1	1.58 ± 0.16	17.3 ± 4.6	22.3 ± 0.2	1.93 ± 0.51	-10.8 ± 2.3
		i	21.9 ± 0.1	1.51 ± 0.12	16.4 ± 0.7	22.3 ± 0.2	1.84 ± 0.45	-11.7 ± 1.9
8	NGC 3753	g	23.6 ± 0.3	3.0 ± 0.59	10.0 ± 2.8	24.7 ± 0.4	2.1 ± 0.08	-15.2 ± 2.1
		r	22.9 ± 0.2	3.08 ± 0.58	8.8 ± 1.4	24.1 ± 0.4	1.93 ± 0.07	-30.0 ± 1.7
		i	22.5 ± 0.3	3.17 ± 0.64	12.3 ± 2.1	22.8 ± 0.2	2.42 ± 0.08	-28.7 ± 1.7
9	UGC 6882	g	22.7 ± 0.3	1.79 ± 0.41	8.3 ± 5.7	22.6 ± 0.3	1.88 ± 0.04	-6.1 ± 0.5
		r	22.3 ± 0.2	2.15 ± 0.48	6.7 ± 4.5	22.2 ± 0.3	2.17 ± 0.05	-4.8 ± 0.5
		i	22.3 ± 0.2	2.46 ± 0.53	10.2 ± 6.4	21.9 ± 0.2	2.29 ± 0.05	-6.7 ± 0.6
10	SDSS J140639.64+272242.4	g	23.3 ± 0.1	2.44 ± 0.04	-5.6 ± 0.3	23.0 ± 0.1	2.21 ± 0.04	6.0 ± 0.3
		r	22.0 ± 0.1	3.07 ± 0.05	-4.5 ± 0.2	21.8 ± 0.1	2.80 ± 0.05	3.8 ± 0.2
		i	22.0 ± 0.1	3.44 ± 0.04	-3.4 ± 0.4	21.3 ± 0.1	2.72 ± 0.04	6.2 ± 0.2
11	SDSS J153538.63+464229.5	g	22.5 ± 0.1	0.92 ± 0.09	3.5 ± 0.1	22.7 ± 0.1	1.52 ± 0.59	-5.9 ± 0.1
		r	22.0 ± 0.1	1.05 ± 0.10	0.2 ± 0.1	22.2 ± 0.1	1.70 ± 0.08	-1.6 ± 0.4
		i	21.9 ± 0.1	1.19 ± 0.12	2.2 ± 0.1	22.0 ± 0.1	1.93 ± 0.10	-6.4 ± 0.1
12	UGC 10716	g	23.5 ± 0.3	1.51 ± 0.04	3.9 ± 0.3	22.9 ± 0.1	1.58 ± 0.35	-0.9 ± 0.2
		r	22.8 ± 0.2	1.76 ± 0.06	4.0 ± 0.4	22.5 ± 0.1	2.24 ± 0.46	-1.0 ± 0.1
		i	22.5 ± 0.3	2.12 ± 0.07	4.1 ± 0.3	22.4 ± 0.3	2.59 ± 0.54	-0.4 ± 0.1
13	UGC 12253	g	22.9 ± 0.1	1.69 ± 0.41	3.6 ± 2.2	23.2 ± 0.2	1.94 ± 0.04	-1.7 ± 0.2
		r	22.3 ± 0.2	2.51 ± 0.55	4.9 ± 2.5	22.7 ± 0.3	2.45 ± 0.06	-1.7 ± 0.2
		i	21.9 ± 0.2	2.47 ± 0.56	4.4 ± 3.3	22.2 ± 0.3	2.52 ± 0.06	-2.2 ± 0.3

5 RESULTS AND DISCUSSION

5.1 Photometric characteristics of galaxies

The mean characteristics of the sample galaxies – $\langle M_r \rangle = -20.51 \pm 1.43$, $\langle g-r \rangle = +0.64 \pm 0.25$, $\langle r-i \rangle = +0.36 \pm 0.18$, $\langle B/T \rangle = 0.16 \pm 0.18$ – are typical for bright edge-on disc-dominated spirals (e.g. Bizyaev et al. 2014). As expected, bulges of our galaxies are redder than their discs: $\langle g-r \rangle_B = +0.91 \pm 0.27$ vs. $\langle g-r \rangle_D = +0.68 \pm 0.26$ and $\langle r-i \rangle_B = +0.60 \pm 0.15$ vs. $\langle r-i \rangle_D = +0.42 \pm 0.14$.

The galaxies show notable radial colour gradients: $\langle h_g/h_r \rangle = 1.15 \pm 0.08$ and $\langle h_g/h_i \rangle = 1.20 \pm 0.13$, where h_g , h_r , h_i – scale lengths of the discs in the g , r and i passbands respectively.

Such gradients are usual for the discs of late-type spirals (e.g. Elmegreen & Elmegreen 1984, de Grijs 1998).

The average disc flattening for the sample is $\langle z_0/h_r \rangle = 0.34 \pm 0.15$ or, excluding four most inclined galaxies (SPRC-192, NGC 3753, UGC 6882 and SDSS J153538.63+464229.5 – see Table 1), $\langle z_0/h_r \rangle = 0.30 \pm 0.11$ (r passband). Both values are somewhat higher as compared to normal spirals of the same morphological types, luminosities and colours (Mosenkov et al. 2015) but, within the quoted scatter, the difference is not significant.

Table 4. Log of spectral observations.

#	Galaxy	Slit PA (deg)	Date	Spectral range (ÅÅ)	Exp. time (s)	Seeing (")
1	IC 194	193	20.11.2014	3650–7250	2×900	1.7
2	2MFGC 6306	164	10.10.2012	3650–7250	5×1200	2.1
3	SPRC 192	98	10.10.2012	3650–7250	5×1200	2.3
		110	08.12.2012	3650–7250	7×900	2.9
4	UGC 4591	14	14.12.2014	3650–7250	6×900	1.0
5	MCG +06-22-041	132	15.12.2014	3650–7250	7×900	1.1
6	NGC 3160	140	24.02.14	3650–7250	6×900	1.3
		150	15.12.2014	3650–7250	4×900	1.1
7	UGC 5791	60	10.12.2012	3600–8500	3×900	2.9
8	NGC 3753	107	06.03.2013	3650–7250	4×1200	1.8
		125	06.03.2013	3650–7250	4×1200	3
9	UGC 6882	120	12.12.2012	3650–7250	4×1200	1.1
		130	12.12.2012	3650–7250	4×1200	1.2
10	SDSS J140639.64+272242.4	140	07.03.2013	3650–7250	5×1200	1.9
11	SDSS J153538.63+464229.5	74	07.03.2013	3650–7250	3×1200	1.5
12	UGC 10716	12	12.07.2013	5700–7500	2×1200	1.4
13	UGC 12253	144	15.12.2014	3650–7250	8×900	1.7

5.2 Kinematical characteristics of galaxies

Fig. 3 presents rotation curves (RCs) of the galaxies averaged with respect to their dynamic centres. Optical RCs of edge-on galaxies are strongly suffered by internal absorption which changes their shapes (e.g. Bosma et al. 1992, Zasov & Khoperskov 2003, Stepanova & Volkov 2013). However, our RCs are sufficiently extended (mean extension of the curves is $(0.80 \pm 0.19) a$, where a is a semi-major axis of the galaxy, see Table 1) to estimate rotational velocities and to check the Tully-Fisher (TF) relation for the sample galaxies.

Following the standard practice, we have fitted RCs by the arctangent function (Courteau 1997, Willick 1999)

$$V(r) = \frac{2}{\pi} V_a \arctan\left(\frac{r}{r_t}\right), \quad (4)$$

where V_a is an asymptotic velocity and r_t is a turnover radius where the rotation curve goes from rising to flat. (For two galaxies with apparently peculiar RCs – 2MFGC 6306 and UGC 4591 – we have used the observed velocities within $r \leq 10''$ in our calculations, for SDSS J153538.63+464229.5 we have took the data within $r \leq 15''$. At larger radii, the spectrograph slit, probably, shifted away from the warped edge-on disc for these galaxies.)

The fitted value V_a can significantly overestimate the true rotation velocity when the observed points do not reach the flat part of the rotation curve. In order to avoid this, the rotation speed at 2.2 disc scale lengths ($V_{2.2}$) is used in our work. To obtain $V_{2.2}$, we find the value of the arctangent function at a distance of $2.2h_r$.

The results of our analysis are summarized in Table 5. For each galaxy the table gives fitted r_t and V_a values, as well as their uncertainties. The last column of Table 5 presents $V_{2.2}$ values corrected for the cosmological broadening.

The Tully-Fisher relation for the sample galaxies is presented in Fig. 4. (For the galaxies with rotation curves obtained at two position angles, we use the larger value of $V_{2.2}$.) As one can see, warped galaxies follow the relation for normal spirals in a wide

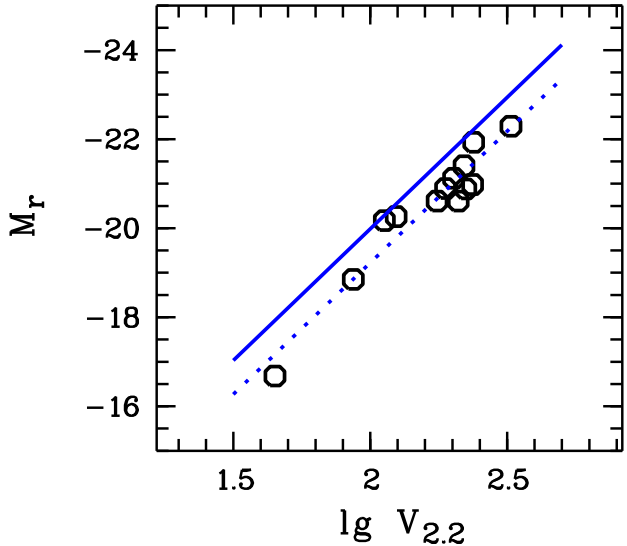


Figure 4. The r band Tully-Fisher relation for edge-on spiral galaxies with warped discs (circles). Solid line represents the TF relation according to Pizagno et al. (2007), dotted line – the same relation shifted by $\Delta M_r = 0.76$.

range of luminosities. The slope of the TF for warped galaxies (-5.99 ± 0.50) is consistent with the slope for usual spirals (-5.91 ± 0.20 – see Pizagno et al. 2007). Some systematic shift of warped spirals towards fainter absolute magnitudes ($\Delta M_r = 0.76$) can be explained by the internal extinction taking place in edge-on spiral galaxies.

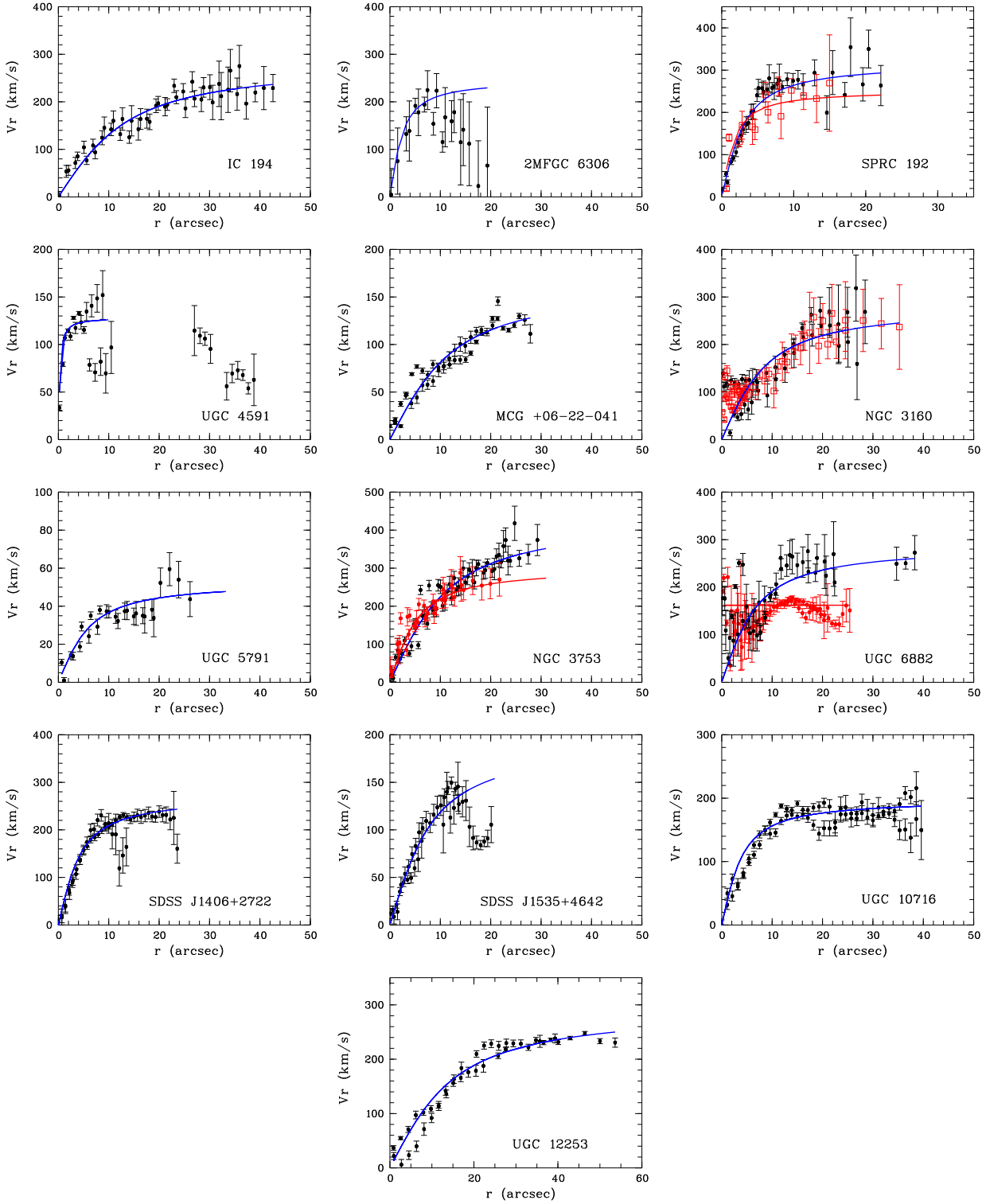


Figure 3. Rotation curves of 13 sample galaxies. Solid curves show the best-fit arctangent functions. **SPRC-192:** black symbols and blue curve correspond to position angle of slit P.A. = 110° , red symbols and red curve – P.A. = 98° ; **NGC 3160:** black symbols – P.A. = 140° , red symbols – P.A. = 149.5° , blue curve gives arctangent fit for joint rotation curve; **NGC 3753:** black symbols and blue curve – P.A. = 107° , red symbols and curve – P.A. = 125° ; **UGC 6882:** black symbols and blue curve – P.A. = 130° , red symbols and curve – P.A. = 120° .

Table 5. Kinematical characteristics of the sample galaxies.

#	Galaxy	r_t ($''$)	σ_{r_t} ($''$)	V_a (km/s)	σ_{V_a} (km/s)	$V_{2.2}$ (km/s)
1	IC 194	11.2	1.3	283	13	223
2	2MFGC 6306	2.2	1.1	247:	30	202:
3	SPRC 192 (PA=110)	2.7	0.3	318	10	239
	SPRC 192 (PA=278)	1.6	0.3	252	13	210
4	UGC 4591	0.3	0.3	128:	10	124:
5	MCG +06-22-041	10.2	1.6	165	10	87
6	NGC 3160	7.4	0.8	282	14	220
7	UGC 5791	5.3	1.3	53	5	45
8	NGC 3753 (PA=107)	9.4	0.8	433	16	326
	NGC 3753 (PA=125)	4.6	0.6	302	14	260
9	UGC 6882 (PA=300)	-	-	162:	4	157:
	UGC 6882 (PA=310)	5.8	0.9	288	13	236
10	SDSS J140639.64+272242.4	3.7	0.3	270	8	188
11	SDSS J153538.63+464229.5	7.0	0.9	194:	15	113:
12	UGC 10716	3.5	0.4	198	4	175
13	UGC 12253	12.5	1.1	293	6	210

Table 6. Characteristics of warps in the g , r , i filters

	North	South	All
$\langle\mu_g\rangle$	22.84 \pm 0.60	22.80 \pm 0.67	22.82 \pm 0.62
$\langle\mu_r\rangle$	22.21 \pm 0.59	22.22 \pm 0.77	22.22 \pm 0.68
$\langle\mu_i\rangle$	22.01 \pm 0.60	21.87 \pm 0.67	21.94 \pm 0.63
$\langle R_{w,g}\rangle$	2.10 \pm 0.65	1.98 \pm 0.33	2.04 \pm 0.51
$\langle R_{w,r}\rangle$	2.38 \pm 0.67	2.30 \pm 0.49	2.34 \pm 0.58
$\langle R_{w,i}\rangle$	2.53 \pm 0.75	2.40 \pm 0.47	2.47 \pm 0.62
$\langle\psi_g\rangle$	7.0 \pm 4.6	7.8 \pm 5.6	7.4 \pm 5.0
$\langle\psi_r\rangle$	6.6 \pm 4.7	8.0 \pm 7.9	7.3 \pm 6.4
$\langle\psi_i\rangle$	7.7 \pm 5.2	9.0 \pm 7.5	8.3 \pm 6.4

Rows:

(1)–(3) average surface brightness where warp starts,

(4)–(6) average projected distance where warp begins (in units of scale length h),

(7)–(9) average warp angle in degrees

5.3 Characteristics of warps

Table 6 presents average characteristics of stellar disc warps in the three filters.

On average, warps start at a projected distance of $\approx 2.5 h$. There is a clear dependence of R_w on a passband (Table 6), but this dependence just reflects the fact that the scale length depends on the colour. The scale lengths are larger in the g filter (Sect. 5.1), therefore, R_w values in units of blue scale lengths are smaller. As for R_w values in absolute units (in arcseconds or in kpc), warps start from about the same projected distance in all three filters: average ratio of the projected distances in the g and r passbands is 1.00 ± 0.09 , in the r and i passbands $- 0.99 \pm 0.07$.

Projected starting points of stellar warps vary among different sources. For example, de Grijs (1997) gives $\langle R_w \rangle = (2.1 \pm 1.0) h$ in the I filter. Ann & Park (2006) studied 325 edge-on galaxies

from the Digitized Sky Survey (DSS) and found that $\langle R_w \rangle = (0.9 \pm 0.3) R_{25}$, where R_{25} is the semi-major axis of the $\mu_B = 25 \text{ mag}/\square''$ isophote. For the standard exponential disc (Freeman 1970) with the central surface brightness in the B filter of $\mu_0 \approx (21 - 22) \text{ mag}/\square''$ this result transforms into $\langle R_w \rangle = (2.5 - 3.3) h$. For ten galaxies observed in the *Spitzer*/IRAC 4.5- μm band, the mean warp radius is $(4.1 \pm 1.0) h$ (Saha, de Jong & Holwerda 2009). Since the disc scale length decreases with wavelength (see e.g. de Grijs 1998; Xilouris et al. 1999), the last estimate of R_w is in general agreement with the values obtained in optical filters.

Fig. 5a shows the observed distribution of warp angles ψ in the north and south sides of galaxies (ψ_N and ψ_S together). As one can see, the warp angles have a relatively wide distribution which extends to $\psi \sim 20^\circ$. Average values of ψ (see Table 6) are large in comparison with the typical values for spiral galaxies (e.g. Sánchez-Saavedra, Battaner & Florido 1990, Reshetnikov & Combes 1998, Ann & Park 2006). Apparently, this can be regarded a consequence of the selection effect, since our sample includes galaxies with perceptible warps only.

There is a tendency for stronger warps to start from a closer distance to the center. This tendency is almost absent in the g band but quite pronounced in the r and i filters. For instance, the mean projected starting point of warp $\langle R_{w,r} \rangle$ for the galaxies with the mean warp angle $\langle \psi_r \rangle < 7^\circ$ is $(2.45 \pm 0.57) h_r$, but for $\langle \psi_r \rangle > 7^\circ$ this value is $(2.10 \pm 0.31) h_r$. The same values in the i -band: $\langle R_{w,i} \rangle = (2.64 \pm 0.57) h_i$ for $\langle \psi_i \rangle < 7^\circ$ and $\langle R_{w,i} \rangle = (2.19 \pm 0.42) h_i$ for $\langle \psi_i \rangle > 7^\circ$. Probably, the dependence in the g filter does not appear due to the influence of the dust extinction on the observable structure of edge-on galaxies.

If we exclude two galaxies in which spiral arms can mimic warps (UGC 6882 and SDSS J153538.63+464229.5), the effect becomes stronger:

$$\langle R_{w,r} \rangle = (2.65 \pm 0.42) h_r \text{ vs. } \langle R_{w,r} \rangle = (2.10 \pm 0.31) h_r \\ (\langle \psi_r \rangle < 7^\circ \text{ and } \langle \psi_r \rangle > 7^\circ, \text{ respectively}) \\ \text{and}$$

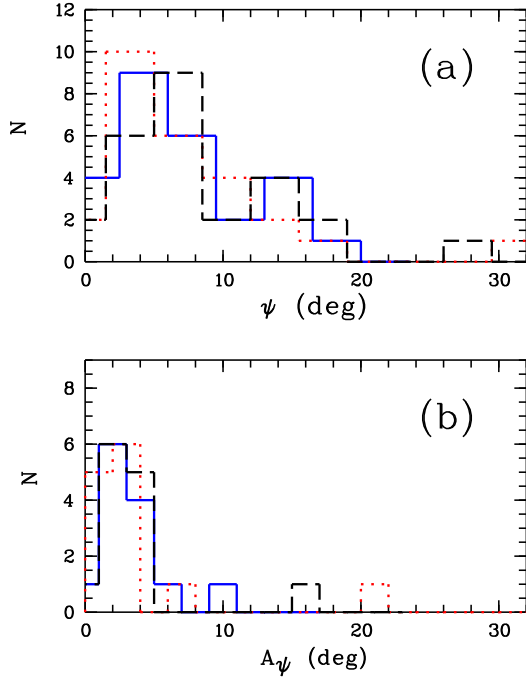


Figure 5. Distributions of the sample galaxies over the warp angle ψ (a) and over the warp asymmetry A_ψ (b). Solid (blue) lines show the distributions in the g passband, dotted (red) – in the r , and dashed (black) – in the i bands.

$\langle R_{w,i} \rangle = (2.79 \pm 0.39) h_i$ vs. $\langle R_{w,i} \rangle = (2.15 \pm 0.47) h_i$ ($\langle \psi_i \rangle < 7^\circ$ and $\langle \psi_i \rangle > 7^\circ$, respectively).

The data presented in Table 6 clearly show that warps measured within the certain isophotes are asymmetric for all galaxies in the sample (partially this may be explained again by the presence of dust lanes). To quantify the observed asymmetry, we used different asymmetry indexes (see García-Ruiz, Sancisi & Kuijken 2002, Castro-Rodríguez et al. 2002, Saha, de Jong & Holwerda 2009). First two indexes provide asymmetry as the difference of ψ and R_w values in two sides of galaxies (both values of ψ must be positive, regardless of the sign in Table 3):

$$A_\psi = |\psi_N - \psi_S| \text{ (in degrees),}$$

$$A_R = |R_{w,N} - R_{w,S}| \text{ (in units of scale length } h).$$

Two other indexes give dimensionless measure of warp (both values of ψ are taken positive):

$$\delta_\psi = \frac{|\psi_N - \psi_S|}{\psi_N + \psi_S} \text{ and } \delta_R = \frac{|R_{w,N} - R_{w,S}|}{R_{w,N} + R_{w,S}}.$$

Table 7 presents average values of the warp asymmetries. As can be seen in the table, typical asymmetries reach several degrees in ψ (see also Fig. 5) and about 50 per cent of the exponential scale length in R_w .

Fig. 6 shows dependence of the relative asymmetry δ_ψ on the average warp angle. As one can see, for larger mean warp angles $\langle \psi \rangle$ we have less relative asymmetry δ_ψ (Fig. 6). This anticorrelation was noted earlier by Castro-Rodríguez et al. (2002) (see fig. 1i in their work). Most likely, this dependence does not have physical sense and just reflects the definition of δ_ψ : assuming that $A_\psi = |\psi_N - \psi_S|$ is restricted within the narrow region, we can expect that $\delta_\psi \propto \langle \psi \rangle^{-1}$. (In fact, for most galaxies $A_\psi \leq 5^\circ$ – see Fig. 5b.)

Table 7. Average warps asymmetries in the g , r , i filters.

	g	r	i
A_ψ	3.3 ± 2.4	4.0 ± 5.4	3.8 ± 4.0
A_R	0.45 ± 0.30	0.45 ± 0.32	0.53 ± 0.33
δ_ψ	0.28 ± 0.18	0.33 ± 0.24	0.30 ± 0.29
δ_R	0.11 ± 0.07	0.10 ± 0.08	0.11 ± 0.06

Rows:

(1)–(2) absolute asymmetries of warp (A_ψ in degrees, A_R in units of scale length h),

(3)–(4) relative warp asymmetries.

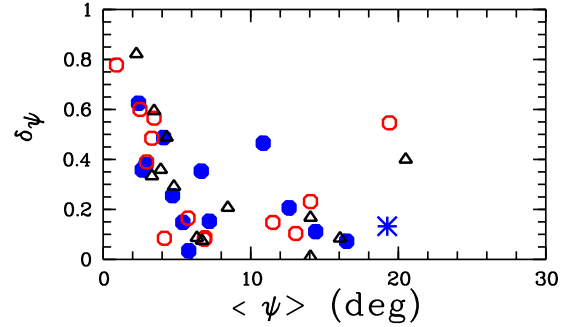


Figure 6. Relative warp asymmetry δ_ψ versus mean warp angle $\langle \psi \rangle$. Solid (blue) circles – g filter, open (red) circles – r filter, open triangles – i filter. Blue asterisk shows characteristics of the famous “integral sign” galaxy UGC 3697 (Ann 2007).

5.4 Dark haloes and optical warps

According to most theoretical models, dark haloes play a significant or even decisive role in the fate of warps. In order to verify the effect of dark halo, we calculate the ratio of the dynamical mass of our galaxies to their stellar mass. The dynamical mass is defined as the total mass enclosed within the sphere of radius $r = 4 h_i$: $M_{tot} = 4 h_i V_{2,2}^2 / G$. The stellar mass was estimated according to Bell et al. (2003) using the $g - r$ colours and r band luminosities of galaxies. The total (dynamical) mass includes the stellar mass of the galaxy (M_*) and the dark halo (M_h). Therefore, $M_{tot}/M_* = (M_h + M_*)/M_* = M_h/M_* + 1$.

Most of the galaxies in the sample (12 of 13) show the M_{tot}/M_* ratio in the range from 1.7 to 6.4 (Fig. 7a) with the mean value $\langle M_{tot}/M_* \rangle = 3.9 \pm 1.9$. These values are in agreement with what was obtained by Mosenkov et al. (2010) for the sample of edge-on spirals with JHK photometry (see fig. 13a in their work). (MCG +06-22-041 is the most dark-matter dominated galaxy in the sample with $M_{tot}/M_* \approx 14$. Rotation curve of this galaxy steeply rises up to the last observational point (Fig. 3). Also, MCG +06-22-041 has unusually blue optical colours – see Table 1.) Fig. 7b illustrates that the sample galaxies follow a trend for the disc flattening with the relative contribution of the dark halo – more dark-dominated galaxies are, on average, thinner (e.g. Zasov et al. 2002).

We have investigated possible correlations of the warp parameters with M_{tot}/M_* ratio. The most promising trends we found are

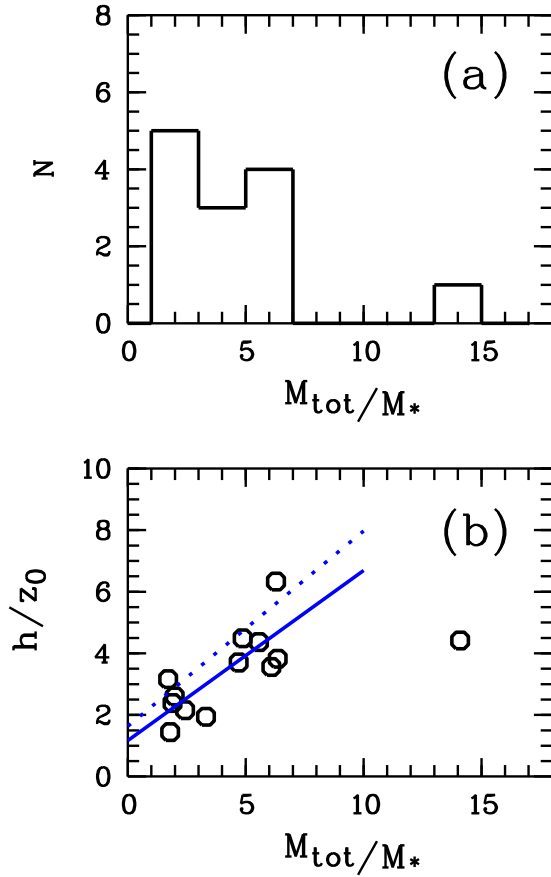


Figure 7. (a) Distribution of the sample galaxies over the ratio of dynamical mass to stellar mass. (b) The ratio of h/z_0 in the r filter as a function of the ratio of dynamical mass to stellar mass. Solid line shows linear regression for the sample galaxies (excluding MCG +06-22-041), dotted line represents the same relation in the J filter according to Mosenkov et al. (2010).

shown in Fig. 8a,b. As one can see that the mean warp angle $\langle\psi\rangle$ and the warp asymmetry A_ψ both decrease with the rise of the dark halo contribution. Large and strongly asymmetric warps are more common among galaxies with relatively less massive haloes. (Several related correlations were presented in Castro-Rodríguez et al. 2002.)

6 CONCLUSIONS

We have performed detailed photometric and kinematic study of the 13 edge-on spiral galaxies with warped stellar discs. The galaxies were selected solely on the basis of their optical morphology and, therefore, they are *a priori* with notable integral-shape warp. As it turned out, most of them reside in dense spatial environments – in pairs, groups, clusters – and, hence, tidal interaction (current or past) with companions may be possible mechanism for the origin of stellar warps in our sample.

Our main conclusions are as follows:

(i) The sample galaxies demonstrate wide distribution of the warp angles ψ , with maximum values of $\psi \sim 20^\circ$ (Fig. 5a).

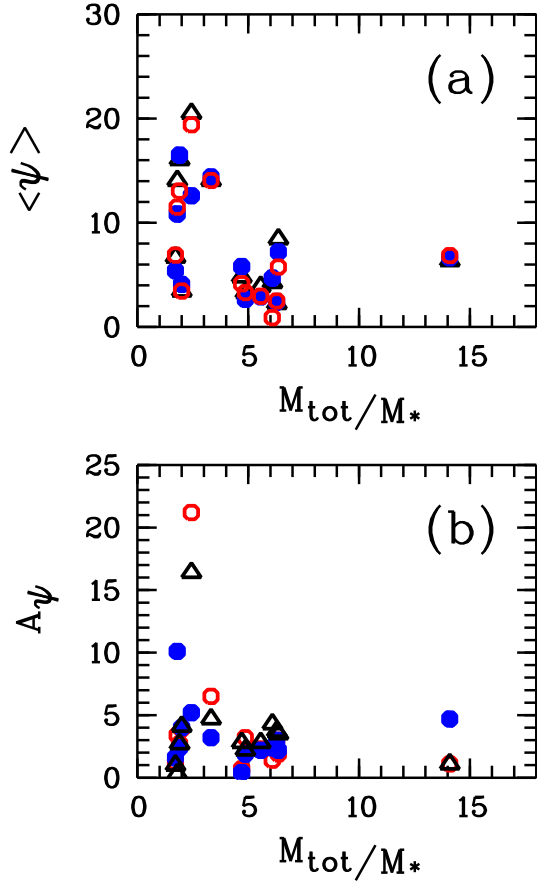


Figure 8. Mean warp angle $\langle\psi\rangle$ (a) and asymmetry of warp $A_\psi = |\psi_N - \psi_S|$ (b) versus the ratio of dynamical mass to stellar mass. Symbols as in Fig. 6. $\langle\psi\rangle$ and A_ψ values are in degrees.

(ii) On average, stellar warps start at a projected distances of $(2-3)h$, i.e. near or just beyond the maximum of the rotation curve of a self-gravitating exponential disc (Table 6).

(iii) Stronger warps have on average a smaller projected starting point (Sect. 5.3).

(iv) Warps show notable asymmetry in all the sample galaxies. Typically, asymmetry reaches several degrees in ψ , about 50 per cent of the exponential scale length in R_w , and about 0.5 mag in μ_w (Tables 3 and 7).

(v) Apparently, as the dark halo becomes more and more massive compared to the stellar disc, it prevents the formation of very strong and asymmetric warps (Fig. 8).

In order to investigate the formation of stellar warps, Kim et al. (2014) recently presented a set of N -body simulations of fly-by encounters between galaxies. They have found that fly-bys can excite integral-shape warps in galaxies, and such induced warps can survive for a few billion years. In Kim et al. (2014) simulations, the maximum warp angle reaches about 25° , and warps are often non-symmetric. These results are quite consistent with our observational data. Significant asymmetry of the projected starting points of warps (Sect. 5.3) could probably arise due to the underlying

asymmetry in the dark halo potential (Saha, de Jong & Holwerda 2009), which could be induced by the galaxy-galaxy interactions.

Our results are based on a small sample of galaxies, and they can only be regarded as preliminary. Also, these results can be biased due to the misidentification of strongly inclined spirals as warped stellar discs. Reshetnikov & Combes (1998) simulated this projection effect and found that no more than $\approx 15\%$ of integral-shaped warps could actually be spiral arms. Careful study of the sample galaxies showed that, with a certain probability, in 2 of 13 galaxies the global warp can be explained as inclined spiral arms (these galaxies are UGC 6882 and SDSS J153538.63+464229.5). Thus, the fraction of possible false warps in the sample is in general agreement with the Reshetnikov & Combes (1998) results. We verified the position of the studied characteristics of these two galaxies in our figures and found that they do not bias our conclusions.

A further extended studies of warped galaxies in different spatial environments will help us to better understand this common but still puzzling phenomenon.

ACKNOWLEDGMENTS

The observations at the 6-meter BTA telescope were carried out with the financial support of the Ministry of Education and Science of the Russian Federation (agreement No. 14.619.21.0004, project ID RFMEFI61914X0004). This work was partly supported by the Russian Foundation for Basic Researches (grant number 14-02-810). Aleksandr Mosenkov is a beneficiary of a mobility grant from the Belgian Federal Science Policy Office. Alexei Moiseev is grateful for the financial support a grant from the President of the Russian Federation (MD-3623.2015.2). We thank Sergey Dodonov, Dmitri Oparin, Roman Uklein and Oleg Egorov, who performed the significant part of SCORPIO/SCORPIO-2 observations and especially Victor Afanasiev for his great contribution to spectroscopy at the 6-m telescope. Also we thank Tatiana Briukhareva for her help in spectral data reduction. We are thankful to the referee for useful comments.

Funding for the SDSS has been provided by the Alfred P. Sloan Foundation, the Participating Institutions, the National Science Foundation, the U.S. Department of Energy, the National Aeronautics and Space Administration, the Japanese Monbukagakusho, the Max Planck Society, and the Higher Education Funding Council for England. The SDSS Web Site is <http://www.sdss.org/>.

We acknowledge the usage of the HyperLeda database. This research has made use of the NASA/IPAC Extragalactic Database (NED) which is operated by the Jet Propulsion Laboratory, California Institute of Technology, under contract with the National Aeronautics and Space Administration.

REFERENCES

- Afanasiev V. L., Moiseev A. V., 2005, *Astron. Lett.*, 31, 194
 Afanasiev V. L., Moiseev A. V., 2011, *Baltic Astron.*, 20, 363
 Alam S., Albareti F.D., Allende Prieto C. et al., 2015, *ApJS*, 219, 12
 Ann H.B., 2007, *JKAS*, 40, 9
 Ann H.B., Park J.-C., 2006, *New Astronomy*, 11, 293
 Battaner E., Florido E., Sanchez-Saavedra M.L., 1990, *A&A*, 236, 1
 Bell E.F., McIntosh D.H., Katz N., Weinberg M.D., 2003, *ApJS*, 149, 289
 Berlind A.A., Frieman J., Weinberg D.H. et al., 2006, *ApJS*, 167, 1
 Bertin E., Arnouts S., 1996, *A&AS*, 117, 393
 Binney J., 1992, *ARA&A*, 30, 51
 Bizyaev D.V., Kautsch S.J., Mosenkov A.V. et al., 2014, *ApJ*, 787, 24
 Bosma A., 1981, *AJ*, 86, 1825
 Bosma A., Byun Y., Freeman K.C., Athanassoula E., 1992, *ApJ*, 400, L21
 Briggs F.H., 1990, *ApJ*, 352, 15
 Bureau, M., Aronica, G., Athanassoula, E., et al. 2006, *MNRAS*, 370, 753
 Caon N., Capaccioli M., D’Onofrio M., 1993, *MNRAS*, 265, 1013
 Castro-Rodríguez N., López-Corredoira M., Sánchez-Saavedra M.L., Battaner E., 2002, *A&A*, 391, 519
 Chilingarian I.V., Zolotukhin I.Y., 2012, *MNRAS*, 419, 1727
 Courteau S., 1997, *AJ*, 114, 2402
 De Geyter G., Baes M., Fritz J., Camps P., 2013, *A&A*, 550, A74
 De Geyter G., Baes M., Camps P. et al., 2014, *MNRAS*, 441, 869
 de Grijs R., 1997, *Edge-on Disk Galaxies – A Structure Analysis in the Optical and Near-Infrared*, PhD thesis, Univ. Groningen, The Netherlands
 de Grijs R., 1998, *MNRAS*, 299, 595
 de Souza R.E., Gadotti D.A., dos Anjos S., 2004, *ApJS*, 153, 411
 Dubinski J., Kuijken K., 1995, *ApJ*, 442, 492
 Elmegreen D.M., Elmegreen B.G., 1984, *ApJS*, 54, 127
 Erwin, P. 2015, *ApJ*, 799, 226
 Florido F., Prieto M., Battaner E., Mediavilla F., Sanchez-Saavedra M.I., 1991, *A&A*, 242, 301
 Freeman K.C., 1970, *ApJ*, 160, 811
 García-Ruiz I., Sancisi R., Kuijken K., 2002, *A&A*, 394, 769
 Goldberg D.E., 1989, *Genetic Algorithms in Search, Optimization, and Machine Learning* (Reading, MA: Addison-Wesley)
 Guíjarro A., Peletier R.F., Battaner E. et al., 2010, *A&A*, 519, A53
 Hickson P., 1982, *ApJ*, 255, 382
 Huang S., Carlberg R.G., 1997, *ApJ*, 480, 503
 Innanen K.A., Kamper K.W., Papp K.A., van den Bergh S., 1982, *A&A*, 254, 515
 Kautsch S.J., Grebel E.K., Barazza, F.D., Gallagher J.S., 2006, *A&A*, 445, 765
 Kemp S.N., Meaburn J., 1993, *A&A*, 274, 19
 Kim J.H., Peirani S., Kim S. et al., 2014, *ApJ*, 789, id.90
 Kuijken K., García-Ruiz I., 2001, *ASP Conference Series*, 230, 401
 Lintott C.J., Schawinski K., Slosar A. et al., 2008, *MNRAS*, 389, 1179
 Lintott C., Schawinski K., Bamford S. et al., 2011, *MNRAS*, 410, 166
 Mitronova S.N., Karachentsev I.D., Karachentseva V.E., Jarrett T.H., Kudrya Y.N., 2004, *Bulletin of the Special Astrophysics Observatory*, 57, 5
 Moiseev A.V., Smirnova K.I., Smirnova A.A., Reshetnikov V.P., 2011, *MNRAS*, 418, 244
 Mosenkov A.V., Sotnikova N.Ya., Reshetnikov V.P., 2010, *MN-*

- RAS, 401, 559
- Mosenkov A.V., 2014, *Astrophysical Bulletin*, 69, 99
- Mosenkov A.V., Sotnikova N.Y., Reshetnikov V.P., Bizyaev D.V., Kautsch S.J., 2015, *MNRAS*, 451, 2376
- Olsen K.A.G., Salyk C., 2002, *AJ*, 124, 2045
- Peng Ch.Y., Ho L.C., Impey Ch.D., Rix H.-W., 2010, *AJ*, 139, 2097
- Patterson F.S., 1940, *Harvard Bull. No.914*, 9
- Pizagno J., Prada F., Weinberg D.H. et al., 2007, *AJ*, 134, 945
- Peterson S.D., 1979, *ApJS*, 40, 527
- Reed B.C., 1996, *AJ*, 111, 804
- Reshetnikov V., 1989, *Astrophysics*, 30, 359
- Reshetnikov V., Combes F., 1998, *A&A*, 337, 9
- Reshetnikov V., Combes F., 1999, *A&AS*, 138, 101
- Reshetnikov V., Battaner E., Combes F., Jiménez-Vicente J., 2002, *A&A*, 382, 513
- Revaz Y., Pfenniger D., 2001, *ASP Conference Series*, 240, 278
- Roškar R., Debattista V.P., Brooks A.M. et al., 2010, *MNRAS*, 408, 783
- Saha K., de Jong R., Holwerda B., 2009, *MNRAS*, 396, 409
- Sánchez-Saavedra M.L., Battaner E., Florido E., 1990, *MNRAS*, 246, 458
- Sánchez-Saavedra M.L., Battaner E., Guijarro A., López-Corredoira M., Castro-Rodríguez N., 2003, *A&A*, 399, 457
- Sancisi R., 1976, *A&A*, 53, 159
- Sandage A., Humphreys R.M., 1980, *ApJ*, 236, L1
- Sasaki T., 1987, *PASJ*, 39, 849
- Schlafly E.F., Finkbeiner D.P., 2011, *ApJ*, 737, 103
- Schwarzkopf U., Dettmar R.-J., 2001, *A&A*, 373, 402
- Sellwood J.A., 2013, *Planets, Stars and Stellar Systems*, 5, 923
- Sérsic J.L., 1968, *Atlas de Galaxias Australes*, Observatorio Astronómico, Córdoba
- Simard L., Willmer C.N.A., Vogt N.P. et al., 2002, *ApJS*, 142, 1
- Sheth K. et al., 2010, *PASP*, 122, 1397
- Sparke L.S., Casertano S., 1988, *MNRAS*, 234, 873
- Spitzer L., 1942, *ApJ*, 95, 325
- Stepanova K.V., Volkov E.V., 2013, *Astronomy Letters*, 39, 405
- Toomre A., 1983, in *Internal kinematics and dynamics of galaxies*, Proceedings of the Symposium, 177
- Trasarti-Battistoni R., 1998, *A&AS*, 130, 341
- van der Kruit P.C., 2007, *A&A*, 466, 883
- van der Kruit P.C., Searle L., 1981a, *A&A*, 95, 105
- van der Kruit P.C., Searle L., 1981b, *A&A*, 95, 116
- van der Kruit P.C., Searle L., 1982a, *A&A*, 110, 61
- van der Kruit P.C., Searle L., 1982b, *A&A*, 110, 79
- White R.A., Bliton M., Bhavsar S.P. et al., 1999, *AJ*, 118, 2014
- Willick J.A., 1999, *ApJ*, 516, 47
- Xilouris, E. M., Byun, Y. I., Kylafis, N. D., Paleologou, E. V., Papamastorakis, J. 1999, *A&A*, 344, 868
- Zasov A.V., Bizyaev D.V., Makarov D.I., Tyurina N.V., 2002, *Astronomy Letters*, 28, 527
- Zasov A.V., Khoperskov A.V., 2003, *Astronomy Letters*, 29, 437